Articles

Cationic 5,10,15,20-Tetrakis(*N*-methylpyridinium-4-yl)porphyrin Fully Intercalates at 5′-CG-3′ Steps of Duplex DNA in Solution†

Anton B. Guliaev‡ and Neocles B. Leontis*

Chemistry Department, Bowling Green State University, Bowling Green, Ohio 43403

Received June 16, 1999; Revised Manuscript Received August 26, 1999

ABSTRACT: The interaction of 5,10,15,20-tetrakis(*N*-methylpyridinium-4-yl)porphyrin ($T4MPyP^{4+}$) with the oligonucleotide DNA duplex $[d(GCACGTGC)]_2$ was studied by two-dimensional ^1H NMR spectroscopy, optical absorbance, circular dichroism, and molecular dynamics simulation employing particle mesh Ewald methods. $T4MPyP^{4+}$ is one of the largest aromatic molecules for which intercalative binding to DNA has been proposed, although this has been called into question by recent X-ray crystallographic work [Lipscomb et al. (1996) *Biochemistry 35*, 2818−2823]. $T4MPyP^{4+}$ binding to $[d(GCACGTGC)]_2$ produced a single set of (mostly) upfield-shifted DNA resonances in slow exchange with the resonances of the free DNA. Intra- and intermolecular NOEs observed in the complex showed that the porphyrin intercalates at the central 5′-CG-3′ step of the DNA duplex without disrupting the flanking base pairs. Absorption and circular dichroism spectra of the complex also support intercalative binding. Molecular dynamics simulations (using explicit solvent and PME methods), carried out for fully and partially intercalated complexes, yielded stable trajectories and plausible structures, but only the symmetrical, fully intercalated model agreed with NOESY data. Stable hydrogen bonding was observed during 600 ps of MD simulation for the base pairs flanking the binding site.

Many antibiotic and antitumor drugs exert their biological effects by intercalative binding to double-helical DNA (*1*). A major challenge in the use of such drugs as antineoplastic agents is to increase their specificity so as to decrease damaging side effects to normal tissues. A promising modality of drug therapy that has recently entered the clinic makes use of compounds whose cytotoxic effects are activated only upon irradiation with light (*2*). The cationic porphyrin *meso*-tetrakis(*N*-methylpyridinium-4-yl)porphyrin ($T4MPyP^{4+}$,[1] Figure 1A) has many favorable properties for photodynamic therapy that potentially may overcome many of the shortcomings of clinically approved, first-generation photosensitizers, including the persistent cutaneous photosensitivity after systemic injection (*3*) and the dependence upon oxygen for photodynamic action. The latter limits the effectiveness of such agents under the hypoxic conditions that quickly develop in tumors during photodynamic treatments (*4, 5*). $T4MPyP^{4+}$ concentrates in the nuclei of cultured cells and, upon irradiation, causes damage to DNA leading to cell death (*6*). $T4MPyP^{4+}$ administered systemically to mice localizes in tumor cells, actively discriminating against normal muscle and epithelial cells and thus minimizing skin photosensitivity (*7, 8*). $T4MPyP^{4+}$ photosensitizes singlet oxygen production with high quantum yield (*9*). Moreover, it directly photosensitizes DNA damage by electron transfer from guanosine bases to the intimately bound photoexcited drug (*10*−*12*). $T4MPyP^{4+}$ is chemically stable, remains monomeric under physiological conditions, and is nontoxic in the absence of light. Understanding the mechanisms of $T4MPyP^{4+}$ binding to DNA and their consequences is thus basic to understanding and exploiting its biological effects.

Intercalation of $T4MPyP^{4+}$ in duplex DNA was first proposed in 1979 (*13*) on the basis of DNA-induced changes in the porphyrin absorption and circular dichroism (CD) spectra and porphyrin-induced increases in the viscosity of linear DNA solutions. The benchmark spectroscopic effects for intercalation include significant red shifting and hypochromicity of the porphyrin Soret absorption band and negative induced circular dichroism signals, also in the Soret band (*10*). Further evidence for DNA intercalation is provided by porphyrin induced unwinding of supercoiled DNA (*14*) and

† This work was supported by grants from the NIH (1R15 GM55898) and the Petroleum Research Foundation (31427-B25). The 400 MHz NMR spectrometer at BGSU Chemistry Department was funded by NSF Grant CHE-9302619 and the circular dichroism spectrometer was funded by NSF Grant BIR-9208356.

* Corresponding author: 419-372-2301; Fax 419-372-9809; Email leontis@bgnet.bgsu.edu.

‡ Present address: Donner Laboratory, LBL, University of California, Berkeley, CA 94720.

[1] Abbreviations: $T4MPyP^{4+}$ or P, 5,10,15,20-tetrakis(*N*-methylpyridinium-4-yl)porphyrin; MD, molecular dynamics; PME, particle mesh Ewald; 2M-2m, DNA complex in which two *N*-methylpyridinium substituents of the porphyrin lie in the major (M) groove of the DNA and two in the minor (m) groove; 3M-1m, DNA complex in which three *N*-methylpyridinium substituents of the porphyrin lie in the major groove and one in the minor groove; 1M-3m, DNA complex in which one *N*-methylpyridinium substituent of the porphyrin lies in the major groove and three in the minor groove).

10.1021/bi9913808 CCC: $18.00
Published on Web 11/05/1999

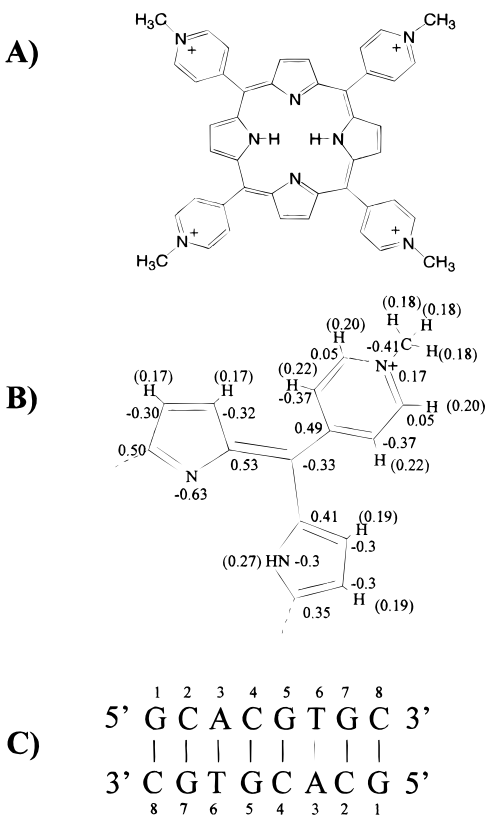

FIGURE 1: (A) Structure of T4MPyP^{4+}. (B) Calculated atom-centered charges for T4MPyP^{4+} employed for MD simulations of T4MPyP^{4+}/DNA complexes. (C) Self-complementary DNA duplex $[d(GCACGTGC)]_2$.

by the slow dissociation kinetics of porphyrin/DNA complexes (*15*).

Three modes of cationic porphyrin binding to DNA have been proposed: intercalation, outside surface (or groove) binding, and outside surface binding with self-stacking (*10*). The binding mode depends on the nature of the *meso*-substituents on the porphyrin, the DNA sequence, the ionic strength, and the presence and nature of metal ions liganded to the porphyrin. As for smaller intercalators, T4MPyP^{4+} prefers 5′-CG-3′ duplex DNA sites, although intercalation has also been proposed at duplex 5′-TG-3′ steps on the basis of kinetic measurements (*16*). T4MPyP^{4+} also groove binds to AT rich sequences with binding constants comparable to those for intercalation (*15, 17*).

A recent X-ray crystallographic study of the Cu(II) complex of T4MPyP^{4+} with the self-complementary DNA oligonucleotide $[d(CGATCG)]_2$ shows two porphyrin molecules bound per DNA duplex molecule, one at each 5′-CG-3′ step, confirming the binding preference noted in solution studies (*18*). Extensive aromatic $\pi-\pi$ stacking interactions occur between the porphine nucleus of the drug and nucleic acid bases (see the Nucleic Acid Database, coordinate file DDF060). Two of the positively charged *N*-methylpyridinium *meso*-substituents are located in the minor groove and two in the major groove of the DNA, and all four interact with the negatively charged DNA backbone. Due to the square planar coordination geometry of the Cu(II) ion, the metal ion does not interfere with intercalation. Nonetheless, the terminal C-G base pairs at each end of the hexamer duplex are disrupted. Each 3′-terminal G stacks on the bound porphyrin, but each 5′-terminal C is extruded from the helix and pairs with the 3′-terminal G of a neighboring DNA molecule in the crystal. The 5′-terminal C of a third molecule base-pairs with the 3′-terminal G of the original duplex and stacks on the porphyrin. Thus, each porphyrin occupies a binding site comprising two π-stacked base pairs, but the terminal pair is composed of bases belonging to different molecules. The authors applied the term hemiintercalation to describe this binding and further suggested that T4MPyP^{4+} should also disrupt one or more base pairs when intercalated to duplex DNA in solution.

^{31}P and ^{1}H NMR solution studies of the binding of cationic porphyrins, including T4MPyP^{4+} and its *ortho* and *meta* isomers, to DNA oligomer duplexes have been reported (*19, 20*) and reviewed (*11*). Intercalation at 5′-CG-3′ steps was inferred from characteristic porphyrin-induced shifts of ^{31}P and G imino proton resonances. However, detailed nuclear Overhauser studies have not yet been reported, and consequently, the questions raised by the crystallographic study regarding the actual structures of T4MPyP^{4+}/DNA complexes in solution remain open.

The large size, multiple binding modes, and high affinities of cationic porphyrins for DNA have attracted the interest of the molecular modeling community. Manual and automated docking followed by energy minimization with various molecular mechanics force fields have been employed to account for the sequence specificity of intercalation vs groove-binding. Ford et al. (*21*) concluded that full intercalation was possible at 5′-CG-3′ sites but not at 5′-TA-3′ duplex sites, due to steric hindrance from thymidine methyl groups. Hui et al. (*22*) proposed three alternative intercalation possibilities for binding at 5′-CG-3′ sites, depending on the number of porphyrin *meso*-substituents located in the major (M) vs the minor (m) groove of the DNA: 1M-3m, 2M-2m, and 3M-1m. Ford and Neidle (*23*) investigated groove binding in AT-rich sequences.

Previous modeling studies were carried out before adequate treatments of long-range electrostatic forces were available. Truncation of the long-range Coulombic forces (to limit the number of pairwise terms that need to be evaluated) leads to unacceptable errors affecting the stability and dynamics of molecular dynamics (MD) simulations of nucleic acids (*24, 25*), even for long cutoffs (16 Å) (*26*). The particle mesh Ewald method provides an excellent approximation to the full electrostatic energy while remaining computationally efficient (*27, 28*). PME permits stable MD simulation of nucleic acids on the nanosecond time scale (*29, 30*) and even reproduces sequence-specific structural effects and conformational transitions (*31, 32*).

In this report, we present optical (absorbance and CD) and 2D NMR data of T4MPyP^{4+} complexed to the DNA duplex $d[(GCACGTGC)]_2$. Alternative molecular models suggested by the NMR data were constructed and subjected to MD simulation by using explicit solvent molecules and particle mesh Ewald (PME) treatment of the electrostatic force. The stability of the trajectories was evaluated and intermolecular proton−proton distances calculated from the trajectories were compared with the NMR data to identify the best model.

MATERIALS AND METHODS

Sample Preparation. DNA samples were obtained from Oligos Etc. (Bethel, ME) and T4MPyP^{4+} from Porphyrin

Products, Inc. (Logan, UT). All solutions were prepared in 20 mM phosphate buffer (pH 7.2) containing 0.05 M NaCl and 0.1 mM EDTA. For NMR measurements, the DNA was dissolved to a duplex concentration of 1.5 mM. DNA duplex concentrations were calculated by using an extinction coefficient $\epsilon_{260} = 1.26 \times 10^5\ M^{-1}\ cm^{-1}$ determined from nearest-neighbor parameters (*33*). Corrections were made for hypochromicity arising from duplex formation, as determined from melting curves. The DNA sample was titrated with porphyrin by removing it from the NMR tube in the dark (to protect the sample from photosensitized strand cleavage) and dissolving lyophilized $T4MPyP^{4+}$ aliquots. NMR spectra were acquired at molar ratios, [$T4MPyP^{4+}$]/[DNA], ranging from 0.25 to 2. $T4MPyP^{4+}$ concentrations were calculated by using the extinction coefficient $\epsilon_{422} = 2.26 \times 10^5\ M^{-1}\ cm^{-1}$ (*15*).

Absorption and CD Spectroscopy. Absorption spectra were recorded on an HP8452A diode-array spectrophotometer. Porphyrin samples (1.0 mL volume, 3.6×10^{-6} M) were titrated in a 10 mm quartz cuvette with aliquots of a concentrated DNA solution. Absorption curves (200−700 nm) were rescaled to compensate for volume changes.

Circular dichroism spectra were obtained on an AVIV and Associates 62DS circular dichroism spectrometer (Lakewood, NJ). The spectrometer was calibrated with an aqueous solution of (1*S*)-(+)-10-camphorsulfonic acid. The spectra (300−600 nm) were obtained with a 1 nm wavelength step as averages of two scans. Porphyrin samples were titrated with DNA, as for the absorption study.

NMR Spectroscopy. All experiments were conducted with a 400 MHz Varian Unity Plus NMR spectrometer having a PFG probe. Water suppression was achieved with the WATERGATE (Water suppression by gradient-tailored excitation) method (*34*). NOESY spectra were acquired in H_2O by time-proportional phase incrementation (TPPI) with these parameters: spectral widths 8000 Hz, 4K complex points in t_2, 512 t_1 increments, 32 scans/increment, 300 ms mixing time, and recycle delay 5.0 s. NMR data were processed with Felix95 (Biosym/MSI, San Diego, CA). Data in both dimensions were zero-filled to 2048 real points and apodized with 75° shifted, squared sine bell functions.

Molecular Modeling. To obtain molecular mechanics parameters for $T4MPyP^{4+}$, ab initio quantum mechanical methods were employed with the Spartan program (Wavefunction, Inc., Irvine, CA). $T4MPyP^{4+}$ porphyrin (Figure 1A) was modeled as two fragments, one of which comprised the porphine nucleus and the other the *N*-methylpyridinium-4-yl pendant groups attached to the *meso* positions of the porphine. Allyl groups were attached (at C2) to the *meso* positions of the porphine to model the sp^2 carbon of the pendant groups, and allyl groups were attached to the *para* positions of the *N*-methylpyridinium-4-yl pendant groups to model the sp^2-hybridized *meso*-carbons of the porphine. The geometries were optimized with Hartree−Fock ab initio methods at the 3-21G basis set level. Atom-centered charges were obtained by fitting the electrostatic potential calculated *ab initio* at the 6-311G** basis set level from coordinates optimized at the 3-21G level using the routines provided by the Spartan program (refer to Figure 1B). Calculated bond distances, bond angles, and torsional angles were very similar to those observed crystallographically for $T4MPyP^{4+}$ (*21*). AMBER atom types were assigned according to published guidelines, and torsional and bond stretching constants were scaled according to bond length (*35*). AMBER topology and parameter files for $T4MPyP^{4+}$ and for the B-DNA duplex $[d(GCACGTGC)]_2$ were generated by using the xLeap module of AMBER 5.0 (*36*).

Starting conformations for the 5′-CG-3′ intercalation site were obtained in two ways: (1) by careful energy minimization of hand-docked structures and (2) by extraction of the crystal coordinates of the binding site of the drug daunomycin (a relatively large intercalator) from a crystal structure of the drug complexed to the DNA duplex $[d(CGTACG)]_2$ (*37*). Similar structures resulted from both procedures. Models for fully (2M-2m) and partially (3M-1m and 1M-3m) intercalated complexes were constructed by hand-docking of the porphyrin.

A rectangular box was added providing at least 10 Å of explicit water molecules around the DNA and sufficient Na^+ counterions to neutralize the combined porphyrin/DNA charge. Molecular dynamics (MD) simulations were carried out by using the SANDER module of AMBER5.0 with SHAKE applied to all hydrogen atoms and 2 fs time steps. A 10 Å cutoff was applied to the Lennard-Jones interactions. Constant pressure was maintained with isotropic scaling. At first, the water box was subjected to a series of equilibration MD runs while the solute was held fixed (*29*, *38*). The equilibration runs began with 1000 steps of minimization and were followed by 20 ps of MD, during which the temperature was slowly raised from 10 to 300 K over 4 ps and was maintained at 300 K for the remaining 16 ps. The size of the box was allowed to change until the water density and pressure converged to the correct values. Subsequent equilibration steps, during which position constraints on solute molecules were gradually relaxed, as well as the final production runs, were done by using the particle mesh Ewald (PME) method to calculate electrostatic interactions (*27*). First, another 20 ps of MD was performed while the solute was still held fixed to fully relax the solvent molecules and to complete the density equilibration. This was followed by a second set of 1000 steps of minimization and 3 ps of MD, carried out with restraints on solute molecules reduced to 25 kcal/mol. Finally, five rounds of 800 steps of energy minimization were performed, during which positional restraints were reduced by 5.0 kcal/mol each round. MD production runs of 600 ps were initiated after the system was heated from 10 to 300 K over 4 ps.

RESULTS

Optical Absorbance and Induced Circular Dichroism Studies. Figure 2 shows spectra obtained by addition of concentrated $[d(GCACGTGC)]_2$ to a fixed amount (initially 3.6×10^{-6} M) of porphyrin. (Spectra were corrected for volume changes, which in all cases were < 5%.) The ratio [DNA]/[P] ranges from 0 to 2.5. DNA induces a large red shift in the Soret band, from $\lambda_{max} = 421$ nm for the free porphyrin to $\lambda_{max} = 444$ nm for DNA-bound porphyrin, and significant hypochromicity of the porphyrin absorption (56% at 421 nm and 33% at the respective values of λ_{max}). Notable is the absence of an isosbestic point. Moreover, the absorption spectra recorded for substoichiometric concentrations of DNA cannot be decomposed into superpositions of the spectra of the free and fully DNA-bound porphyrin (obtained

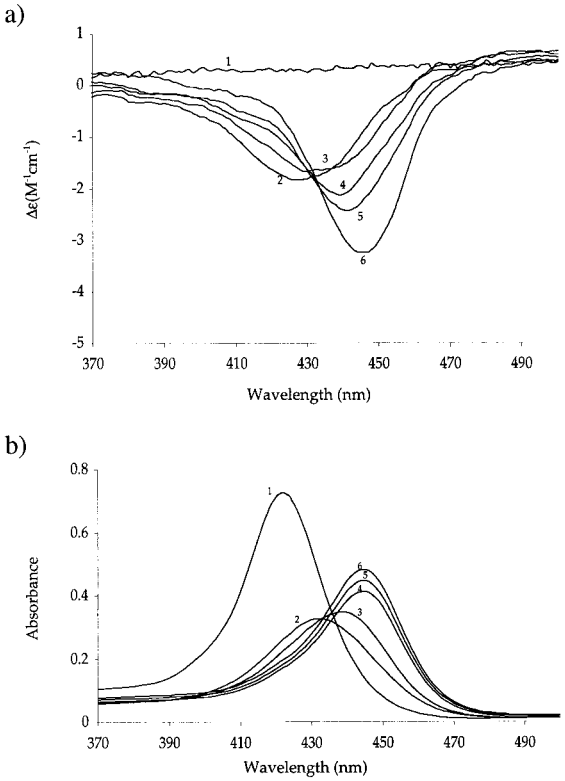

FIGURE 2: Induced circular dichroism spectra (a) and absorption spectra (b) of the Soret region of $T4MPyP^{4+}$ as a function of added DNA duplex $[d(GCACGTGC)]_2$ at constant $[T4MPyP^{4+}] = 3.6 \times 10^{-6}$ M. Spectra were acquired for [DNA]/[P] ratios (1) 0.0, (2) 0.2, (3) 0.5, (4) 1.0, (5) 1.5, and (6) 2.5. The spectra were taken in 20 mM sodium phosphate (pH = 7) and 50 mM NaCl.

at saturating amounts of DNA). Instead, absorption spectra having a single λ_{max} intermediate in value between 421 and 444 nm are observed for [DNA]/[P] < 1.

In the absence of DNA, no CD signal is observed for the optically inactive porphyrin. At [DNA]/[P] = 0.2, a negative induced CD band with $\lambda_{max} = 428$ nm appears (Figure 2). As the [DNA]/[P] ratio increases, the negative intensity of the induced CD band increases and the band shifts toward the red, reaching a value of 444 nm, identical to λ_{max} in the absorption spectra of samples having [DNA]/[P] ≥ 1.0 (Figure 2, curves 3−6).

Large shifts in λ_{max} and substantial hypochromicities in porphyrin absorption spectra, accompanied by large, negative induced CD signals, have been associated with intercalative binding to DNA (*16*, *39*−*41*). On the other hand, small red shifts and hypochromicities accompanied by small, positive induced CD bands indicate surface binding. "Conservative" induced CD bands (exhibiting positive and negative features of approximately equal area) have been associated with porphyrin self-stacking that can be induced by DNA at low values of [DNA]/[P] (*42*). The absence of a definite isosbestic point in the absorption spectra indicates that the porphyrin molecule is binding to $[d(GCACGTGC)]_2$ in two or more distinct sites or modes. At low [DNA]/[P] ratios, the unique intercalation site on the DNA may be saturated, so that excess porphyrin has to bind to the DNA surface. DNA-induced porphyrin aggregation is also a possibility. Thus, the absorption and CD spectra observed at ratios [DNA]/[P] < 1.0 are composite and comprise contributions from specifically bound and surface-bound porphyrin, and possibly also aggregated states. Addition of excess DNA shifts the equilibrium so that most of the porphyrin occupies the unique, specific site giving rise to the $\lambda_{max} = 444$ nm absorption and CD features. Two-dimensional NOESY spectra, reported below, were obtained under conditions of excess DNA ([DNA]/[P] ≥ 1). Detailed evidence for competition between intercalative and aggregative binding modes for $T4MPyP^{4+}$/DNA interactions has been presented for polymeric DNA (*42*−*44*).

Electrophoresis Experiments. Native gel electrophoresis was carried out on 1:1 complexes of $T4MPyP^{4+}$/$[d(GCACGTGC)]_2$. The porphyrin molecule comigrated with the DNA oligonucleotide duplex, indicating that it remained bound to the DNA during electrophoresis (data not shown). In previous work, nonintercalating porphyrins (such as $T2MPyP^{4+}$ or TMAP) that are known to surface- or groove-bind to duplex DNA were shown to dissociate from the DNA during electrophoresis carried out under identical conditions (*45*). Thus, the gel electrophoresis experiments, as well as the absorption and CD studies, provide evidence for tight, intercalative-type binding of $T4MPyP^{4+}$ to the oligonucleotide duplex $[d(GCACGTGC)]_2$. This encouraged us to pursue NMR studies of the interaction.

^{1}H NMR Resonance Assignments and Molecular Modeling of the DNA Duplex $[d(GCACGTGC)]_2$. The proton resonances of the palindromic DNA duplex $[d(GCACGTGC)]_2$ were assigned from homonuclear 2D NOESY and TOCSY spectra (*46*) and are listed by nucleotide, starting from the 5′-end, in the first column of Table 1.

NOE intensities were extracted and used for structure refinement of the DNA duplex using a simulated annealing protocol (*47*−*49*). Restrained molecular dynamics (rMD) were carried out with 10 different starting structures, each of which converged to essentially the same structure (RMSD range ≤ 1 Å). The resulting structure was submitted to 600 ps of unrestrained molecular dynamics (MD) to test our protocols before they were applied to DNA/porphyrin complexes. The conformational dynamics of the DNA over the last 300 ps were analyzed by using the Curves, Dials and Windows program (*50*). The dihedral angle δ at the interior of the furanose sugar ring and ϕ, the pseudorotation angle, were used to monitor the sugar pucker, which for most nucleotides resided primarily in the C1′-exo and C2′-endo conformations. The local helicoidal parameter X-displacement (XDP), which is critical for differentiating canonical B-form (XDP = −0.71 Å) from A-form (XDP = −5.43 Å) DNA, remained between −1.0 and −0.5 Å over the entire 300 ps of free MD, well within the B-conformation range. The analysis showed that the average conformation obtained from free MD belongs to the B-DNA family and does not differ significantly from the structure obtained by rMD (RMSD 1.5 Å).

1D NMR of DNA−$T4MPyP^{4+}$ Complex. One-dimensional spectra of a titration of $[d(GCACGTGC)]_2$ with $T4MPyP^{4+}$ are shown in Figure 3. Addition of porphyrin induced a new set of mostly upfield-shifted DNA resonances. The intensities of resonances of uncomplexed DNA decreased correspondingly. Porphyrin also induced significant line-broadening of DNA resonances, even at the lowest [P]/[DNA] ratio (1:4). For example, at 5 °C, addition of porphyrin to a [P]/[DNA] ratio of 1:2 increased the line width of the methyl resonance of T6 from 7.5 Hz to about 20 Hz. The broadening is likely

Table 1: Chemical Shifts of Proton Resonances of Free and T4MPyP^{4+}-Bound DNA Duplex [d(GCACGTGC)]$_2$ at 5 °C[a]

	imino/amino			H6/H8			H5/H2/Me		
		with T4MPyP^{4+} in solution			with T4MPyP^{4+} in solution			with T4MPyP^{4+} in solution	
nucleotide	DNA without T4MPyP^{4+}	unbound DNA	bound DNA	DNA without T4MPyP^{4+}	unbound DNA	bound DNA	DNA without T4MPyP^{4+}	unbound DNA	bound DNA
G1				7.96	7.96	7.96			
C2	6.60/8.51			7.47	7.47	7.47	5.42	5.42	5.42
A3				8.31	8.30	**8.02**	7.75		
C4	6.60/8.20	6.61/8.20	**5.73/7.73**	7.26	7.26	**7.08**	5.26	5.26	**4.76**
G5	12.80			7.86	7.86	**7.69**			
T6	13.90			7.17	7.17	**6.94**	1.42	1.42	**1.18**
G7	12.90			7.96					
C8	6.67/8.25			7.48			5.49		

	H1′			H3′			H4′		
		with T4MPyP^{4+} in solution			with T4MPyP^{4+} in solution			with T4MPyP^{4+} in solution	
nucleotide	DNA without T4MPyP^{4+}	unbound DNA	bound DNA	DNA without T4MPyP^{4+}	unbound DNA	bound DNA	DNA without T4MPyP^{4+}	unbound DNA	bound DNA
G1	5.93	5.93	5.93	4.82			4.21		
C2	5.59	5.59	**5.60**	4.88	4.87	**4.75**	4.22	4.23	4.23
A3	6.23	6.23	**5.91**	5.06	5.06	**4.98**	4.46	4.46	**4.29**
C4	5.56	5.56	**4.81**	4.82	4.81	**5.42**	4.44	4.43	**4.28**
G5	5.93	5.93	**5.46**	4.92	4.93	**4.82**	4.36	4.36	**4.35**
T6	5.74	5.72	**5.29**	4.84	4.84	**4.80**	4.34	4.34	**4.28**
G7	5.92	5.93		4.92			4.34		
C8	6.19			4.47			4.22		

	H5′/H5″			H2′			H2″		
		with T4MPyP^{4+} in solution			with T4MPyP^{4+} in solution			with T4MPyP^{4+} in solution	
nucleotide	DNA without T4MPyP^{4+}	unbound DNA	bound DNA	DNA without T4MPyP^{4+}	unbound DNA	bound DNA	DNA without T4MPyP^{4+}	unbound DNA	bound DNA
G1	3.69			2.60	2.60	2.60	2.76	2.76	2.76
C2	4.14	4.13	4.14	2.15	2.15	**2.13**	2.45	2.45	**2.34**
A3	4.07/4.17	4.07/4.17	**4.12**	2.74	2.72	**2.47**	2.91	2.91	**2.69**
C4	4.15/4.25	4.15/4.25	**3.41**	2.00	1.99	**2.15**	2.35	2.35	**2.77**
G5	4.07/4.16	4.04/4.13	**3.93/3.73**	2.59	2.60	**2.39**	2.76	2.77	**2.59**
T6	4.15	4.12	**4.18**	2.01	2.02	**1.93**	2.40	2.40	**2.19**
G7	4.11			2.59	2.60		2.75		
C8	4.04			2.17			2.18		

[a] Resonance assignments for DNA in porphyrin-free solution are shown in the first column of each block, and for unbound and bound DNA in the presence of T4MPyP^{4+}, in the second and third columns. Boldface type highlights resonances shifted by porphyrin binding.

due to both the slower tumbling of the complex relative to the duplex and to exchange of drug between DNA and solution or between competing sites on the DNA.

The relative amounts of free and specifically bound DNA were monitored at the well-resolved T6 methyl resonance, which resonates at 1.42 ppm in free DNA and 1.18 ppm in the complex (indicated by the arrow in Figure 3). At [P]/[DNA] = 1:2, the relative intensities of the T6 methyl resonances indicate that roughly equal concentrations of specifically bound DNA and of free (or nonspecifically bound) DNA are present in the solution. However, further increase of the [P]/[DNA] ratio to 1:1 did not saturate the binding. Even at a ratio of 1.5:1 there was still an observable amount of free or nonspecifically bound DNA. This suggests that nonspecific binding sites compete with the specific site that gives rise to distinct resonances, as also suggested by the optical studies.

NOESY Spectra of T4MPyP^{4+}/DNA Complex. NOESY experiments were carried out at [P]/[DNA] ratios of 0.25, 0.35, 0.5, 1.0, and 2.0. For [P]/[DNA] < 0.5, NOEs were too weak to be useful, whereas NOEs could not be observed above ratios of 1:1 due to line broadening. Likewise, for mixing times < 200 ms, NOEs in the complex were too weak to be analyzed. The best NOESY spectra were those acquired at [P]/[DNA] ratios 1:2 and 1:1, and the following discussion concerns these spectra. Representative regions of these spectra, acquired at 5 °C and [P]/[DNA] = 1:2 and 1:1, are shown in Figures 4, 5, 6, and 8.

The NOESY spectra confirmed that the upfield-most resonance at 1.18 ppm corresponds to the methyl group of T6 in the porphyrin/DNA complex. This resonance will be referred to as cT6-Me, whereas T6-Me indicates the corresponding resonance in the unbound DNA. The aromatic−sugar methylene (H2′/H2″) region of the (1:2) NOESY spectrum is shown in Figure 4, and the aromatic−H1′ region is shown in Figure 5. In Figures 4 and 5, NOE connectivities belonging to unbound DNA are traced with black lines and NOE connectivities in the porphyrin/DNA complex are traced with dashed lines. The NOE connectivities for unbound DNA are identical to those observed in the absence of porphyrin. For the complex, sequential NOEs expected for B-form DNA are observed for nucleotides cG1−cC4 and between cG5 and cT6. The resonances of residues cA3, cC4, cG5, and cT6 are significantly shifted relative to uncomplexed DNA and could thus be unambiguously assigned. Although the cC2-H6 resonance is not shifted, it can be

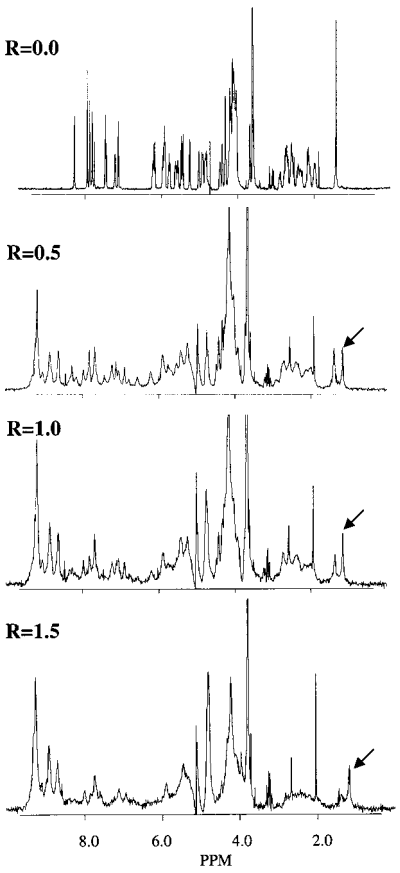

FIGURE 3: ^{1}H NMR titration of the DNA duplex [d(GCACGTGC)]$_2$ by T4MPyP^{4+} (R = [T4MPyP^{4+}]/[DNA]). The upfield-shifted T6 methyl resonance of T4MPyP^{4+}/[d(GCACGTGC)]$_2$ complex is indicated by an arrow.

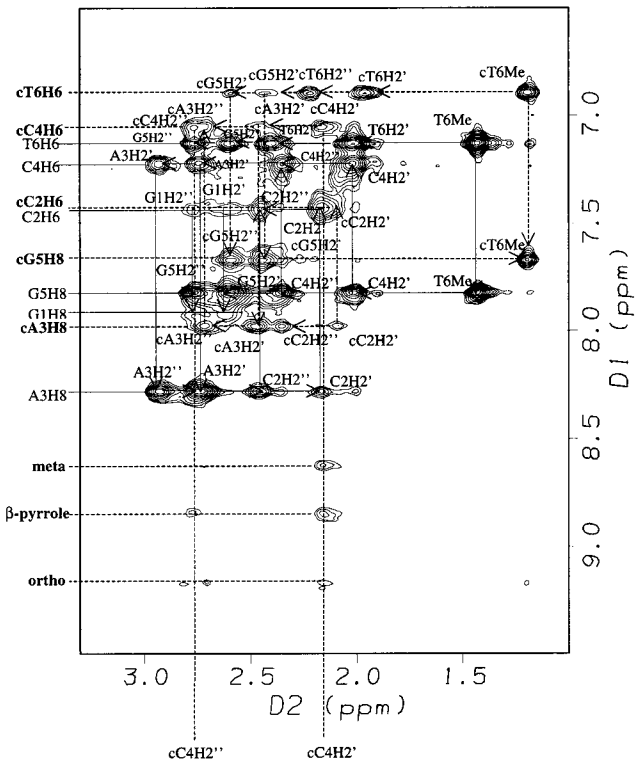

FIGURE 4: NOESY aromatic−methylene sugar region for [T4MPyP^{4+}]/[DNA] = 1/2, acquired at 5 °C in 95% H_2O/5% D_2O with 300 ms mixing time. Solid lines indicate the NOE connectivities for the unbound DNA and dashed lines indicate those of the P/DNA complex. Cross-peaks due to complex are preceded with c. Intermolecular NOEs occur in the lower region of the spectrum.

assigned from NOEs to its own H1′, H2′, and H2″ resonances, which do show small shifts. These resonances can be assigned in turn by their NOEs to the cA3-H8 resonance, which is well separated from that of A3-H8. The cG1 resonances appear to be unshifted relative to free DNA.

Sequential B-form NOEs are observed in the uncomplexed DNA between G5-H8 and the sugar protons of C4 (Figure 5) and between the aromatic protons of C4 and G5. None of these NOEs are observed in the porphyrin/DNA complex. Aromatic−aromatic NOEs are observed, however, between cG5-H8 and cT6-H6 and between cA3-H8 and cC4-H6 in the complex (Figure 6 right panel). Note that even for [P]/[DNA] = 1:1 (rightmost panel of Figure 6), aromatic−aromatic cross-peaks due to unbound (or nonspecifically bound) DNA are still observed. Evidence for additional binding modes, possibly involving terminal bases, is also provided by the lack of observable NOEs involving cG7 and cC8 (Figures 4 and 5). Even at [P]/[DNA] = 1:2, these nucleotides exhibit extremely broad resonances. In summary, sequential NOEs are observed in the porphyrin-bound DNA, but these are interrupted at the C4-G5 step. Specific NOEs from cC4 and cG5 to bound porphyrin resonances appear in place of the sequential C4-G5 NOEs, as discussed below.

Kinetics of Binding. The severe line-broadening of G7 and C8 resonances in the presence of porphyrin may be due to secondary porphyrin-binding sites exhibiting fast to intermediate exchange kinetics, consistent with surface or groove binding. Slow exchange kinetics characterize porphyrin binding to the specific C4/G5 site, as we observe separate sets of peaks for bound and free porphyrin and DNA. An upper limit on the rate of exchange, k_{ex}, for the specific site can be estimated on the basis of the smallest observed chemical shift difference, $\Delta = 0.02$ (for cC2-H2′ vs C2-H2′), between corresponding resonances for free and porphyrin-bound DNA (*51*). This gives an upper limit $k_{ex} \ll \pi\Delta/\sqrt{2} = 17\ s^{-1}$. The rates measured by stopped-flow methods for the dissociation of T4MPyP^{4+} from poly[d(GC)] are among the slowest observed for intercalators, with $k_{ex} = 1.8\ s^{-1}$ (*15*). By contrast, the rate of dissociation of T4MPyP^{4+} from poly[d(AT)] is too fast to measure, even by temperature-jump methods, consistent with surface or groove binding. Thus, the present NMR observations of slow exchange kinetics support intercalative binding for the specific binding of T4MPyP^{4+} to [d(GCACGTGC)]$_2$.

NMR Chemical Shift Changes in P/DNA Complexes. The proton NMR chemical shifts of free and porphyrin-bound DNA are compared in Table 1. The first column in each block gives DNA chemical shifts in the absence of porphyrin; the second column, "unbound" DNA in the presence of porphyrin; and the third column, porphyrin-complexed DNA. The chemical shifts of "unbound" DNA are very close to those of free DNA but may nonetheless represent an equilibrium between free and surface- or groove-bound states, as suggested by the severe broadening of the terminal nucleotides (see above). Despite the line broadening, most of the proton resonances of residues G1−G7 in the bound DNA are resolved and could be assigned from spectra such as those shown in Figures 4 and 5.

The chemical shift differences between free and porphyrin-complexed DNA are plotted as a function of nucleotide

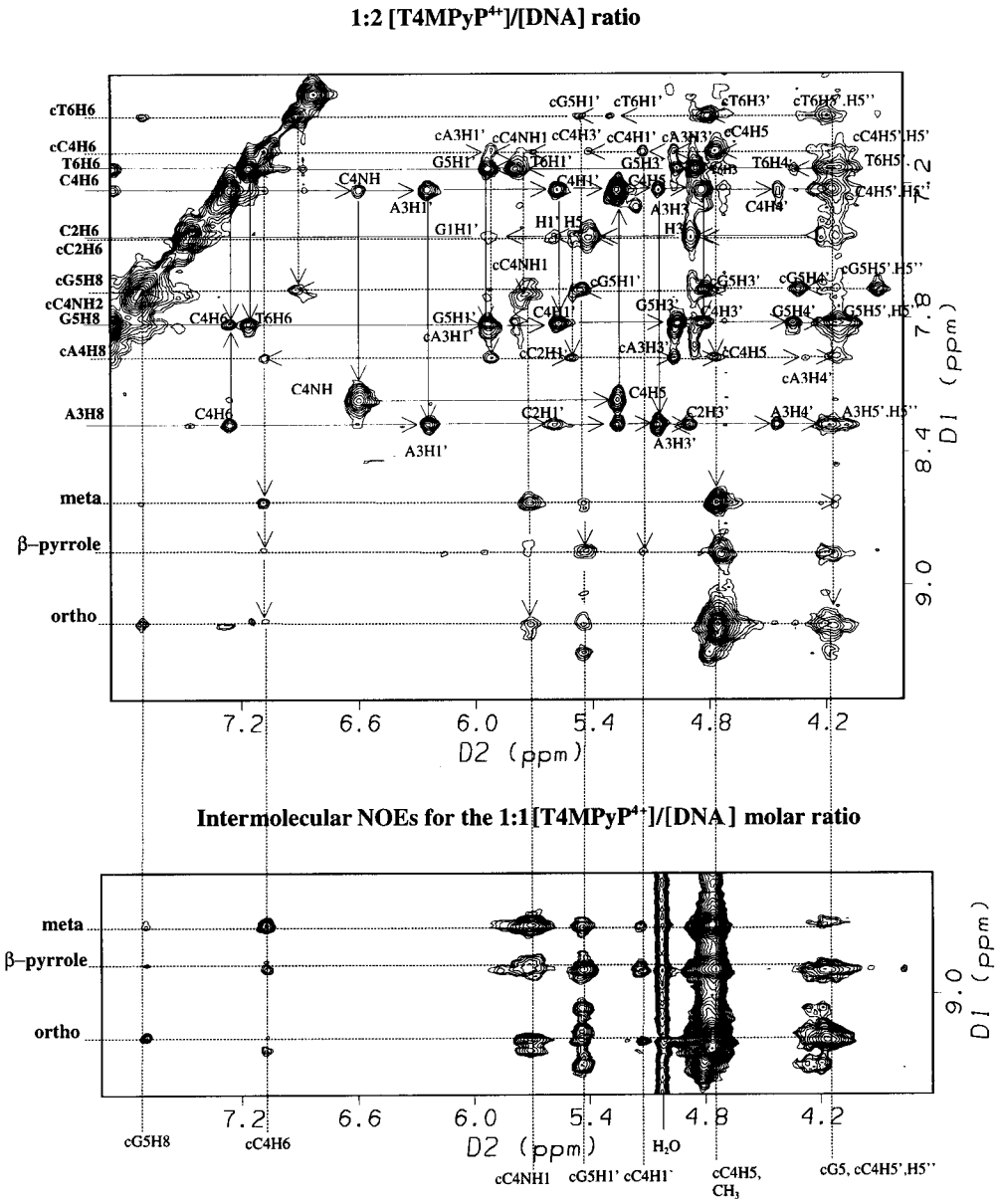

FIGURE 5: Aromatic−H1′/H5/H3′ region of the NOESY spectrum shown in Figure 4. Top panel, [T4MPyP^{4+}]/[DNA] = 1/2; lower panel, [T4MPyP^{4+}]/[DNA] = 1/1. Solid lines indicate the NOE connectivities for the unbound DNA, and dashed lines and letters indicate those of the P/DNA complex. Intermolecular NOEs occur in the lower part of each spectrum.

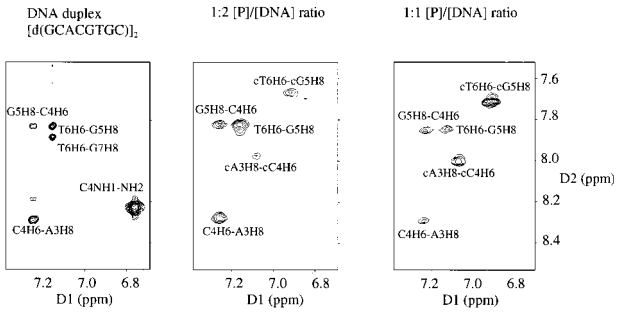

FIGURE 6: Intramolecular aromatic−aromatic NOEs for A3-C4-G5-T6 for free DNA and T4MPyP^{4+}/[d(GCACGTGC)]$_2$ complex. Spectra were acquired at 5 °C in 95% H_2O/5% D_2O with 300 ms mixing time.

position in Figure 7. Large chemical shift changes occur for residues A3−T6 in the middle of the duplex, especially for the central C4 and G5 nucleotides. The proton resonances of C4 exhibit the largest chemical shift changes (0.88 ppm for the non-hydrogen-bonded amino proton, N4-H1, 0.75 ppm for H1′, and 0.47 ppm for N4-H2, the amino proton H-bonded to G5-O6). The chemical shift changes for the H1′ resonances of G5 and T6 are also large (Figure 7). The only downfield-shifted resonances are those of C4-H2′, H2", and H3′. The largest change occurs for C4−H3′ (0.61 ppm, downfield). The clustering of the largest shifts around the central 5′-CG-3′ base step and the presence of a single set of porphyrin-induced DNA resonances indicates symmetrical binding of the drug at the C4-G5 site with respect to the two strands of the duplex. The size of the shifts indicates intimate association of the porphyrin with the C4 and G5 bases of both strands, i.e., intercalation at the 5′-CG-3′ step. The shifts induced by T4MPyP^{4+} binding are at least as large as those observed for other intercalators, consistent with its macrocyclic aromatic structure. For example, the known intercalator 4′-6-diamidino-2-phenylindole (DAPI) produces upfield shifts no greater than 0.25 ppm for aromatic and H1′

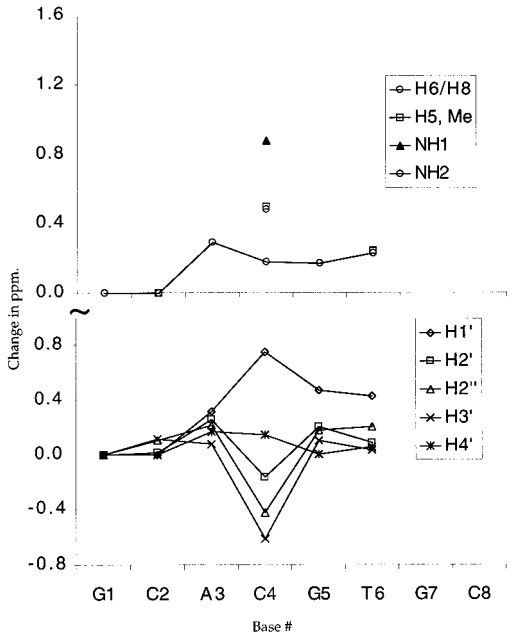

FIGURE 7: Changes in chemical shifts of DNA protons induced by T4MPyP^{4+} binding DNA as a function of nucleotide position. Assignments are from NOESY spectra acquired at 5 °C (Table 1).

proton resonances at the CG site in $[d(GCACGTCG)]_2$ (*52*, *53*). Shifts induced by groove binding drugs are generally smaller (*54*, *55*). The DNA protons that are most likely located in the shielding cone of the porphyrin experience upfield chemical shifts. This includes all assigned G5 and C4 (except H2′, H2″, and H3′) protons as well as the protons of adjacent bases. The large downfield shifts of the H2′, H2″, and H3′ sugar protons of C4 (0.14 ppm for cC4-H2′, 0.42 ppm for cC4-H2″, and 0.61 for cC4-H3′) suggests that they are located at the edge of the porphine nucleus, outside of the shielding cone.

Porphyrin NMR Resonances. Free T4MPyP^{4+} exhibits a simple proton NMR spectrum, owing to fast exchange of its two imino protons, which makes the four pyrrole nitrogens magnetically equivalent. The protons of the four *N*-methyl groups produce a singlet resonating at 5.00 ppm, the *meta* and *ortho* protons of the meso-substituents give rise to doublets at 8.95 and 9.35 ppm, and the β-pyrrole protons of the porphine ring give a singlet at 9.10 ppm (*56*).

DNA binding lifts the 4-fold symmetry of the porphyrin, although some spectral degeneracy of the porphyrin proton resonances may remain, depending on the symmetry of the binding site, the degree of rotational freedom of the substituents, and the similarity of the local environments experienced by protons made inequivalent by binding. In a totally asymmetric binding site (such as that observed in the crystal structure), all symmetry-related protons would potentially have different chemical shifts. If the 2-fold symmetry of the DNA helix is retained upon porphyrin binding, as in the present case, two, three, or even four sets of resonances may be expected for the β-pyrrole protons, depending on the binding mode (2M-2m, 3M-1m, or 1M-3m). For the protons of the methylpyridinium *meso*-substituents, two or three symmetry-related sets of resonances can be expected if the substituents rotate freely. For the most symmetric binding, 2M-2m, two sets of resonances are possible (four if *meso*-substituent rotation is hindered). In the presence of the DNA

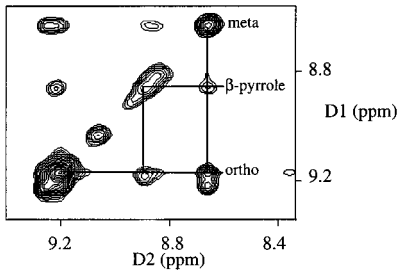

FIGURE 8: Aromatic−aromatic region of NOESY spectrum from Figure 4, showing intramolecular NOEs of T4MPyP^{4+}.

([P]/[DNA] = 1:2), we observe six aromatic resonances attributable to the porphyrin (8.67, 8.88, 8.95, 9.08, 9.18, and 9.26 ppm; see Figure 8). Three of these have the same chemical shifts as unbound porphyrin (8.95, 9.08, and 9.26 ppm), have narrow line widths, and show no intramolecular NOEs. (No NOEs are observed at 400 MHz for the free porphyrin in solution on account of its intermediate molecular weight, 820 g/mol.) The other three signals (8.67, 8.88, and 9.18 ppm) are actually composite peaks that have larger line widths and give both intra- and intermolecular NOEs (Figures 4, 5, and 8). The intramolecular NOEs were used to assign these resonances. The most intense NOE cross-peak occurs between the 8.67 and 9.18 ppm resonances, while the weakest occurs between 8.67 and 8.88 ppm (Figure 8). The most intense NOE was therefore assigned to the *ortho* and *meta* protons on the same methylpyridinium substituent. The distance between these protons is fixed and short (2.48 Å). The distance between any given *ortho* proton and the nearest β-pyrrole proton (about 2.7 Å, depending on torsional angle) is shorter than the corresponding distance between a given *meta* proton and the nearest β-pyrrole proton (about 4 Å). Thus, the weakest intraporphyrin NOE in the P/DNA complex was assigned to the *meta* and β-pyrrole resonances. Intense cross-peaks occur between the *ortho* and *meta* resonances in the complex and a resonance at 4.78 ppm that can be assigned to the CH_3 groups of the same methylpyridinium substituent (Figure 5). Thus DNA binding shifts all porphyrin resonances about 0.20 ppm upfield. The chemical shifts, however, occur in the same order: *ortho* protons (9.18 ppm in complex vs 9.35 ppm for free porphyrin), downfield of β-pyrrole (8.88 ppm in complex vs 9.10 ppm for free), downfield of *meta* (8.67 ppm in complex vs 8.95 ppm for free).

Intermolecular NOEs. NOEs are observed only between bound porphyrin and cC4 and cG5 resonances (Figures 4 and 5). NOEs to bound porphyrin can be resolved for cG5-H8 and cG5-H1′ (but not cG5-H2′ or H2″), and for cC5-H5, H6, H1′, H2″, H2′, and the amino proton cC4-N4(H1). Intermolecular NOEs are also observed to the H5′ and H5″ region of the DNA spectrum but cannot be assigned to individual protons (Figure 5). NOEs are observed to porphyrin *ortho*, *meta*, and β-pyrrole resonances. The strongest intermolecular NOE observed for cG5-H8 is to an *ortho* porphyrin resonance, whereas for cC4-H6 it is to a *meta* resonance. An *ortho* to cC4-H6 cross-peak is also observed, but the *ortho* resonance occurs at a slightly different chemical shift than for the cG5-H8 NOE. The *ortho* proton that has an NOE to cC4-H1′ is also shifted slightly. The cG1-H1′ and the cC4-N4(H1) protons both give NOEs to at least two *ortho* resonances (lower panel of Figure 5). These observa-

tions suggest that specific porphyrin resonances occupy magnetically inequivalent environments and that chemical exchange is not fast enough to average these sites completely. It is, therefore, unlikely that the porphyrin as a whole rotates within the binding site. Rotation of the bound porphyrin substituent groups may also be hindered (as also indicated by MD simulations). Nonetheless, it was not possible to assign the resonances of each of the inequivalent *ortho*, *meta*, and β-pyrrole protons in the complex, because the chemical shift differences were too small and the number of NOEs was too few. Without such assignments, quantitation of intermolecular NOEs was not considered meaningful and restrained MD refinement was not possible.

The intensities of NOEs increased as the [P]/[DNA] ratio was increased from 1:2 to 1:1 (Figure 5), but no additional intermolecular NOEs were observed. High [P]/[DNA] ratios resulted in severe line broadening, making NOEs impossible to observe, while long mixing times were required at lower concentrations of porphyrin to observe NOEs. Intermolecular NOEs could only be observed at long mixing times (>250 ms), giving rise to spin diffusion effects. Nonetheless, intermolecular NOEs only occur between porphyrin and resonances of cC4 and cG5, thus localizing the primary binding site to the C4-G5 step.

In summary, the NMR data indicate that T4MPyP^{4+} binds by intercalating in the center of the duplex with minimal disruption of base pairing. In brief:

(1) T4MPyP^{4+} binding induces one new set of proton resonances in the DNA, indicating that the 2-fold rotational symmetry of the duplex is retained in the complex.

(2) Sequential intra-DNA NOEs (aromatic−sugar and aromatic−aromatic) are observed in the complex, indicating that intrastrand base stacking is retained and is only interrupted at the central 5′-C_4G_5-3′ step.

(3) Porphyrin binding produces large, mostly upfield-directed chemical shifts in DNA base and sugar resonances, consistent with $\pi-\pi$ interactions between the porphyrin macrocycle and the C4 and G5 DNA bases of both strands. The ring currents of the DNA bases induce significant upfield chemical shifts in porphyrin resonances.

(4) Intermolecular NOEs occur only between porphyrin and C4 or G5. NOEs involve DNA resonances in both the major and minor grooves, consistent with "fully threaded" intercalation of the porphyrin into the DNA helix.

(5) Both amino protons of C4 are observed in the complex and show the characteristic difference in chemical shift due to basepairing. Thus, C-G base pairs flanking the binding site are not disrupted by porphyrin binding in solution.

Model Building and MD Simulation of P/DNA Complexes. Three models for T4MPyP^{4+} intercalation in duplex DNA (1M-3m, 2M-2m, and 3M-1m), differing only in the positions of the porphyrin *meso*-substituents relative to the DNA strands, were constructed by hand-docking and extensive energy minimization and equilibration (see Materials and Methods). Free MD trajectories (600 ps) were generated at 300 K for fully solvated structures and PME to calculate electrostatic forces. Trajectories were sampled every 0.5 ps and examined visually by using VMD (*57*). For all three structures, all bases remained paired throughout the simulations, including the C-G pairs flanking the porphyrin binding sites. Analysis of local DNA helicoidal and backbone torsional angle parameters showed that B-form geometry was generally retained in the models except at the intercalation step.

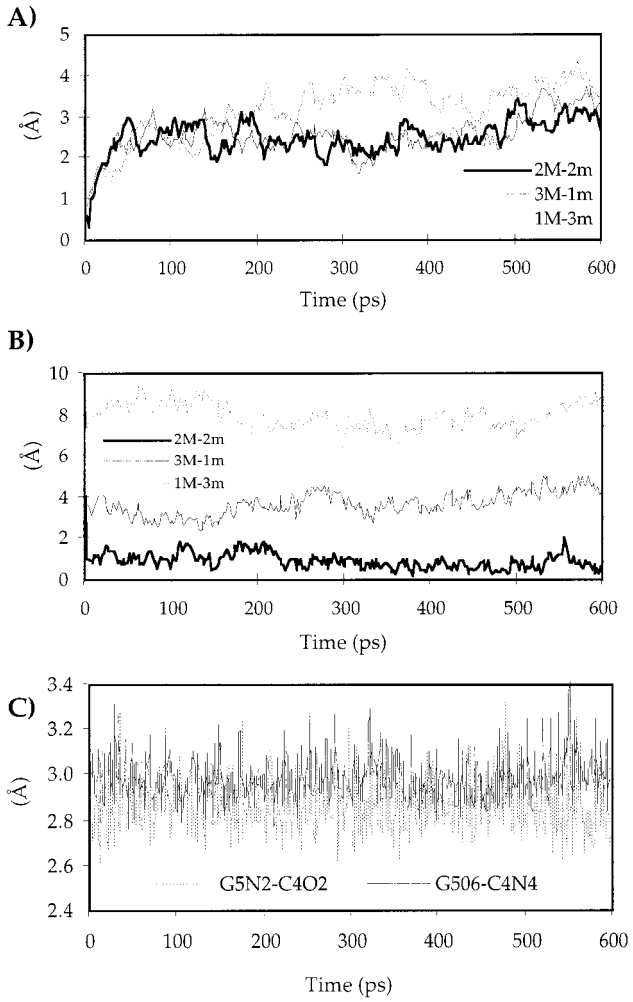

FIGURE 9: (A) Time dependence of RMSD of atomic coordinates of indicated T4MPyP^{4+}/[d(GCACGTGC)]$_2$ complexes relative to energy-minimized starting structures for 600 ps of unrestrained MD. B) Time dependence of distances between the T4MpyP^{4+} and DNA centers of mass for indicated T4MPyP^{4+}/[d(GCACGTGC)]$_2$ complexes. C) Time dependence of representative hydrogen-bond distance for a C4-G5 base pair in the 2M-2m complex during 600 ps of free MD.

The overall stability of each trajectory was evaluated by calculating average RMSD values of each 0.5 ps "snapshot" relative to the coordinates of the initial (energy-minimized) structures. Plots of the average RMSD values as a function of time are shown in Figure 9A. After the initial heating to 300K, the RMSD values remain stable for all three complexes, although a statistically significant, smaller average RMSD was measured for 2M-2m (2.1 ± 0.5 Å) as compared to 3M-1m (2.6 ± 0.5 Å) and 1M-3m (3.2 ± 0.7 Å).

The average distance between the porphyrin and DNA centers of mass was also monitored for each trajectory. The deviations in these values are all quite small and indicate that each porphyrin is docked to the DNA in a stable local minimum (Figure 9B). Only the symmetrically bound 2M-2m complex, however, shows good $\pi-\pi$ interactions between the porphyrin nucleus and the base pairs at the binding site, consistent with the large chemical shift changes observed for both major- and minor-groove protons in the NMR

spectra. The distance separating the porphyrin and DNA centers of mass is significantly smaller for 2M-2m (0.9 ± 0.4 Å for 2M-2m, 3.64 ± 0.6 Å for 3M-1m, and 8.0 ± 0.6 Å for 1M-3m).

Although most relevant, total energies cannot be compared for fully solvated structures, because they are dominated by solvent−solvent interactions. We therefore stripped away all solvent molecules and focused on the two C-G base pairs flanking the binding site to calculate internal and binding energies for the three complexes. This calculation showed that the total potential energy for the 2M-2m binding site (porphyrin and flanking base pairs) is much smaller (95 kcal/mol less than for 1M-3m and 250 kcal/mol less than for the 3M-1m complex). The other structures gave significantly larger covalent bond energies than 2M-2m and smaller intermolecular van der Waals energies.

A crucial test of the fully intercalated 2M-2m model is the stability of the C4-G5 base pairs flanking the porphyrin binding site. The lengths of all hydrogen bonds mediating base-pairing were monitored over 600 ps of MD simulation (Figure 9C). The average GN1−CN3 (imino−imino) H-bond distances were 2.98 ± 0.09 and at no point during the simulations did these values exceed 3.5 Å. The average GO6−CN4 H-bond lengths were 2.88 ± 0.11 Å, and the average GN2−CO2 lengths were 2.96 ± 0.15 Å. Thus, base-pairing remained intact during the simulation. Note that the force field used does not impose artificial H-bond constraints but relies exclusively on the electrostatic forces to calculate the interaction. The rotation of *meso*-substituents was monitored during simulations. In 2M-2m, all substituents only showed fluctuations about their initial values. On the other hand, for 3M-1m complex, the substituent protruding into the major groove showed larger fluctuations and passed twice over the smaller 90° energy barrier.

Comparison of MD Simulations to NMR Data. Although the chemical shifts of the porphyrin proton resonances are well-resolved by type (*ortho*, *meta*, *β*-pyrrole, and *N*-methyl) in both the free and DNA-bound state, resonances could not be assigned to individual protons in the complex. Thus, it was not possible to carry out conventional NOE-based restrained refinement for the porphyrin/DNA complex. Therefore, we chose to compare the MD simulations to the NMR data in the following way: Distances were calculated from the MD trajectories between DNA protons and the nearest porphyrin proton of the type for which an NOE was observed. This was done for each of the three models for the P/DNA complex, 1M-3m, 2M-2m, and 3M-1m (Figure 10). The analysis was carried out over the last 300 ps of the 600 ps MD simulations. The results are presented in Table 2.

The best agreement between the NOESY data and average intermolecular distances from MD was obtained for the 2M-2m model. In 2M-2m, all of the MD-averaged distances for which intermolecular NOEs are observed are less than 5 Å, short enough to account for experiment (*46*). In the 2M-2m conformation, the *meso*-substituents are located near the phosphate−sugar backbone in both major and minor grooves of the DNA. The C4-H5, -H6, and -N4 amino protons and the G5-H8 proton of each strand are within NOE distance of one of the two equivalent *meso*-substituents in the major groove, while the C4-H2′, -H2″, and -H1′ and the G5-H1′ protons of each strand are within NOE range of one of the two equivalent substituents in the minor groove of the DNA. The DNA protons displaying upfield-shifted chemical shifts are all located "above" the porphyrin plane, in the shielding cone of the porphyrin ring currents. On the other hand, the atoms corresponding to the three downfield-shifted resonances, cC4-H2′, -H2″, and -H3′, are located near the edge of the porphyrin macrocycle and nearly coplanar to it, where the ring current-induced magnetic field has the opposite sign. The distance from cC4-H3′ to the closest porphyrin proton is greater than 5 Å in the 2M-2m model, and, in fact, no NOE is observed between cC4-H3′ and $T4MPyP^{4+}$. The 5′ to 3′ orientation of the base pairs in the duplex brings the porphyrin in closer contact to the C4 sugar moiety than to the sugar of G5, resulting in many more intermolecular NOEs for C4 sugar protons.

The 3M-1m model correlates poorly with the NOESY data (Table 2). For example, the MD-averaged distances between G5-H1′ and the closest *meta* and *ortho* protons, located in the minor groove of the DNA duplex, are 7.2 ± 0.5 and 7.1 ± 0.4 Å, respectively, much longer than the corresponding distances in the 2M-2m model. Moreover, no efficient spin-diffusion pathway is evident in the model to account for the observed NOEs involving the G5-H1′ proton. Also, the distance between the nearest *β*-pyrrole proton of the porphine ring and G5-H1′ is longer (5.0 ± 0.3 Å) than in the 2M-2m model (4.0 ± 0.4 Å), as is also the *β*-pyrrole to C4−H5 distance (5.1 ± 0.5 Å in the 3M-1m model vs 4.5 ± 0.5 Å in the 2M-2m model).

For the 1M-3m model, the distances between porphyrin protons and C4-H5, C4-H6, and G5-H8 of either strand are significantly larger than the 5 Å threshold value. For example, the average distances between C4-H5 and the closest *meta*, *ortho*, and *β*-pyrrole porphyrin protons are 5.9 ± 0.3, 7.9 ± 0.4, and 9.1 ± 0.4 Å, respectively. The H1′ of C4 is also too far away from the *β*-pyrrole of the porphine ring to give an observable NOE. The G5-H8 of each strand is between 6.2 Å and 7.2 Å distant from the closest porphyrin protons. In the 1M-3m model the major groove substituent is too far from the DNA protons for which NOEs are observed.

DISCUSSION

The present work provides the most extensive NMR evidence that $T4MPyP^{4+}$ does in fact intercalate into duplex DNA in solution and does so without major disruption of the DNA double helix. Moreover, the NMR data are sufficiently detailed to indicate that the symmetrical (2M-2m) intercalation model is the correct one, at least for binding at 5′-CG-3′ duplex steps. This conclusion is supported by realistic molecular dynamics simulation.

By contrast, X-ray crystallography showed that, at least in a crystal environment, $T4MPyP^{4+}$ binding to the oligonucleotide $[d(CGATCG)]_2$ disrupts the terminal base pair flanking the 5′-CG-3′ binding site, leading to extrusion of the 5′-terminal cytosine (*18*). One explanation for the crystal result is that the porphyrin, due to its large size, generates steric and/or bond strain at the DNA binding site when it is fully intercalated. In the X-ray structure, the binding site was located at the terminal base pair step. Perhaps if the binding site were located in the interior of the duplex, base extrusion would not occur in the crystal. Oligonucleotide duplexes with

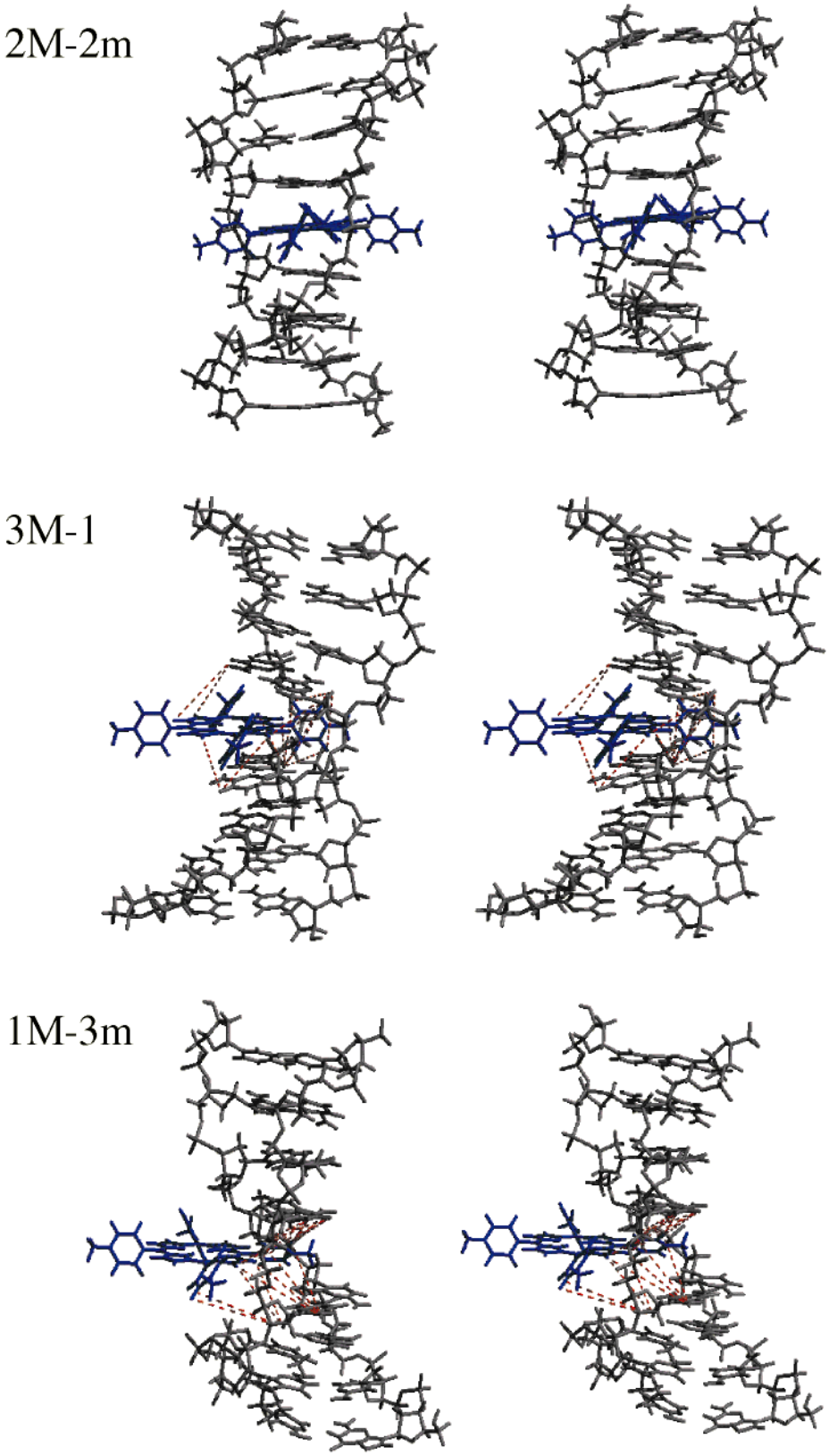

FIGURE 10: Stereo representations of three models for T4MPyP^{4+} intercalation at the C4-G5 step of the DNA duplex d(GCACGTGC)]$_2$. The distances corresponding to observable NOEs exceeding 5 Å in the given model are drawn as red dotted lines. In the case of 2M-2m, all distances are less than 5 Å. For 1M-3m only the distances exceeding 5 Å between one of the symmetry-related strands of the DNA and the porphyrin are drawn, to avoid cluttering the figure. The porphyrin is drawn in blue.

internally located intercalation sites may provide more realistic models for drug interactions with polymeric DNA in solution.

In the crystal, the 5′-terminal cytosine of each strand is extruded from the duplex and forms an otherwise normal cis Watson−Crick base pair with the 3′-terminal G of a

Table 2: Comparison of Average Distances (and Their Deviations) between Protons of C4 and G5 of $[d(GCACGTGC)]_2$ and the Closest $T4MPyP^{4+}$ Protons of the Indicated Type[a]

DNA/$TMPyP^{4+}$ protons		minor groove			major groove		
		meta	*ortho*	β-pyrrole	*meta*	*ortho*	β-pyrrole
				2M-2m Conformation			
cytosine	H5				3.6 ± 0.4	3.2 ± 0.4	5.1 ± 0.5
	H6				4.7 ± 0.5	4.4 ± 0.5	4.5 ± 0.4
	H1′	3.7 ± 0.3	2.4 ± 0.3				3.0 ± 0.4
	H2′				5.4 ± 0.8	5.0 ± 0.7	3.7 ± 0.4
	H2″	4.7 ± 0.7	3.9 ± 0.6				2.9 ± 0.5
	NH1	4.3 ± 0.4	3.0 ± 0.4				4.5 ± 0.4
guanine	H8				4.7 ± 0.4	3.7 ± 0.5	3.8 ± 0.4
	H1′	4.5 ± 0.4	4.3 ± 0.4				4.0 ± 0.4
				3M-1m Conformation			
cytosine	H5				$4.4_{\pm 0.8}$	4.4 ± 0.7	5.5 ± 1.0
	H6				3.5 ± 0.6	3.8 ± 0.6	5.2 ± 0.7
	H1′	4.8 ± 0.4	3.6 ± 0.3				4.7 ± 0.4
	H2′	5.2 ± 0.6	4.9 ± 0.4				4.0 ± 0.5
	H2″	5.2 ± 0.6	4.9 ± 0.5				3.6 ± 0.6
	NH1	4.1 ± 0.3	4.3 ± 0.4				4.7 ± 0.4
guanine	H8				3.8 ± 0.4	3.3 ± 0.5	4.8 ± 0.5
	H1′	7.2 ± 0.5	7.1 ± 0.4				5.0 ± 0.3
				1M-3m Conformation			
cytosine	H5			9.1 ± 0.4	5.9 ± 0.3	7.9 ± 0.4	
	H6			8.1 ± 0.4	5.7 ± 0.3	7.1 ± 0.3	
	H1′			8.2 ± 0.4	4.3 ± 0.8	5.2 ± 0.6	
	H2′			5.2 ± 0.5	4.8 ± 0.4	5.4 ± 0.6	
	H2″			6.0 ± 0.6	4.6 ± 0.3	4.7 ± 0.5	
	NH1			4.3 ± 0.5	4.7 ± 0.7	4.8 ± 0.5	
guanine	H8			6.1 ± 0.4	6.2 ± 0.5	7.1 ± 0.5	
	H1′	5.1 ± 0.3	4.9 ± 0.6	3.0 ± 0.4			

[a] Calculated from 600 ps MD Simulations of the 2M-2M, 3M-1M, and 1M-3m Intercalation Models. Distances were calculated only for DNA protons giving NOEs to the porphyrin.

neighboring molecule in the crystal lattice. Additional stabilizing intermolecular contacts are provided by coaxial stacking between adjacent DNA molecules. None of these interactions is possible in solution. Interestingly, in the crystal, each extruded cytosine stacks on the neighboring porphyrin in a way that is very similar to the stacking of C4 of each strand in our 2M-2m model for the intercalation in $[d(GCACGTGC)]_2$. Thus, the same favorable DNA−base/porphyrin stacking interactions, as well as similar, favorable electrostatic interactions between the porphyrin substituents and the DNA backbone, occur in the solution model as are observed in the crystal. For both the 2M-2m solution model and the crystal structures, the porphyrin is sandwiched between two cis Watson−Crick C-G base pairs.

In addition to direct evidence for specific intercalation of the porphyrin molecule at the 5′-CG-3′ site, the NMR data provide indirect evidence for binding at less-specific surface sites, in agreement with the optical data. Although some of these sites may have comparable binding affinities, their binding kinetics are much faster, in agreement with previous work (*15*, *17*). The fast exchange rate, combined with the much smaller effect of surface-bound porphyrin on DNA proton chemical shifts, makes direct NMR study of these other binding modes very difficult, if not impossible. Although the sequence used also contains a 5′-TG-3′ step, the present NMR data provide no indication for intercalation at this site, at least not in a sequence that provides a competing 5′-CG-3′ intercalation site. The present work thus shows that $T4MPyP^{4+}$ discriminates between 5′-CG-3′ and 5′-TG-3′.

The present work shows that realistic MD simulations can be carried out with the AMBER5.0 force field on DNA−drug complexes by using explicit solvent molecules and PME to accurately account for long-range electrostatic interactions. Accurate calculation of electrostatics is crucial for simulating highly charged ligands such $T4MPyP^{4+}$ interacting with nucleic acid polyelectrolytes. The careful simulation protocols employed generated realistic and stable trajectories that could be independently correlated with experimental data.

ACKNOWLEDGMENT

We thank Dr. Stephen Neidle (U.K.) for the crystallographic coordinates of $T4MPyP^{4+}$, Dr. D. Y. Chen for assistance with NMR spectroscopy, and Pascal Auffinger for critical reading of the manuscript.

REFERENCES

1. Searle, M. S. (1996) in *NMR in Drug Design* (Craik, D. J., Ed.) pp 377−421, CRC Press, Boca Raton, FL.
2. Dougherty, T. J., Gomer, C. J., Henderson, B. W., Jori, G., Kessel, D., Korbelik, M., Moan, J., and Peng, Q. (1998) *J. Natl. Cancer Inst. 90*, 889−905.
3. Dougherty, T. J. (1993) *Photochem. Photobiol. 58*, 895−900.
4. van Geel, I. P., Oppelaar, H., Rijken, P. F., Bernsen, H. J., Hagemeier, N. E., van der Kogel, A. J., Hodgkiss, R. J., and Stewart, F. A. (1996) *Br. J. Cancer 73*, 288−93.
5. Henderson, B. W., and Fingar, V. H. (1989) *Photochem. Photobiol. 49*, 299−304.
6. Villanueva, A., Juarranz, A., Diaz, V., Gomez, J., and Canete, M. (1992) *Anticancer Drug Des. 7*, 297−303.
7. Villanueva, A., and Jori, G. (1993) *Cancer Lett. 73*, 59−64.
8. Villanueva, A., Caggiari, L., Jori, G., and Milanesi, C. (1994) *J. Photochem. Photobiol. B 23*, 49−56.
9. Verlhac, J. B., Gaudemer, A., and Kraljic, I. (1983) *Nouv. J. Chim. 8*, 401.
10. Fiel, R. J. (1989) *J. Biomol. Struct. Dyn. 6*, 1259−1275.
11. Marzilli, L. G. (1990) *New J. Chem. 14*, 409−420.

12. Pasternack, R. F., and Gibbs, E. J. (1996) *Met. Ions Biol. Syst. 33*, 367−97.
13. Fiel, R. J., Howard, J. C., Mark, E. H., and Gupta, N. D. (1979) *Nucleic Acids Res. 6*, 3093−3118.
14. Fiel, R. J., and Munson, B. R. (1980) *Nucleic Acids Res. 8*, 2835−2842.
15. Pasternack, R. F., Gibbs, E. J., and Villafranca, J. J. (1983) *Biochemistry 22*, 5409−17.
16. Gibbs, E. J., Maurer, M. C., Zhang, J. H., Reiff, W. M., Hill, D. T., Malicka-Blaszkiewicz, M., McKinnie, R. E., Liu, H.-Q., and Pasternack, R. F. (1988) *J. Inorg. Biochem. 32*, 39−65.
17. Pasternak, R. F., Garrity, P., Davis, C. B., Gibbs, G., Orloff, G., Giartosio, A., and Turano, C. (1986) *Nucleic Acids Res. 14*, 5919−5931.
18. Lipscomb, L. A., Zhou, F. X., Presnell, S. R., Woo, R. J., Peek, M. E., Plaskon, R. R., and Williams, L. D. (1996) *Biochemistry 35*, 2818−23.
19. Banville, D. L., Marzilli, L. G., and Wilson, W. D. (1983) *Biochem. Biophys. Res. Commun. 113*, 148−154.
20. Marzilli, L. G., Banville, D. L., Zon, G., and Wilson, W. D. (1986) *J. Am. Chem. Soc. 108*, 4188−4192.
21. Ford, K. G., Pearl, H. G., and Neidle, S. (1987) *Nucleic Acids Res. 15*, 6553−6562.
22. Hui, X., Gresh, N., and Pullman, B. (1990) *Nucleic Acids Res. 18*, 1109−1114.
23. Ford, K. G., and Neidle, S. (1995) *Biorg. Med. Chem. 6*, 671−677.
24. York, D. M., Darden, T. A., and Pedersen, L. G. (1993) *J. Chem. Phys. 99*, 8345−8348.
25. Smith, P. E., and Petitt, B. M. (1991) *J. Chem. Phys. 95*, 8430−8441.
26. Auffinger, P., and Beveridge, D. L. (1995) *Chem. Phys. Lett. 234*, 413−415.
27. Darden, T. A., York, D., and Pedersen, L. G. (1993) *J. Chem. Phys. 98*, 10089−10092.
28. Essmann, U., Perera, L., Berkowitz, M. L., Darden, T., Lee, H., and Pedersen, G. (1995) *J. Chem. Phys. 103*, 8577−8593.
29. Cheatham, T. E., Miller, J. L., Fox, T., Darden, T. A., and Kollman, P. A. (1995) *J. Am. Chem. Soc. 117*, 4193−4194.
30. York, D. M., Yang, W., Lee, H., Darden, T. A., and Pedersen, L. G. (1995) *J. Am. Chem. Soc. 117*, 5001−5002.
31. Cheatham, T. E., Miller, J. L., Spector, T. I., Cieplak, P., and Kollman, P. (1998) in *Molecular Modeling of Nucleic Acids* (Leontis, N. B., and SantaLucia, J., Eds.) pp 285−303, American Chemical Society, Washington, DC.
32. Beveridge, D. L., Young, M. A., and Sprous, D. (1998) in *Molecular Modeling of Nucleic Acids* (Leontis, N. B., and SantaLucia, J., Eds.) pp 260−284, American Chemical Society, Washington, DC.
33. Puglisi, J. D., and Tinoco, I., Jr. (1989) *Methods Enzymol. 180*, 304−25.
34. Piotto, M., Saudek, V., and Sklenar, V. J. (1992) *J. Biomol. NMR 2*, 661−665.
35. Cornell, W. D., Kollman, P. A., and Ferguson, D. M. (1995) *J. Am. Chem. Soc. 117*, 5179−5191.
36. Case, D. A., Pearlman, D. A., Caldwell, J. W., Cheatham, T. E., Ross, W. S., Simmerling, C. L., Darden, T. A., Merz, K. M., Stanton, R. V., Cheng, A. L., Vincent, J. J., Crowley, M., Ferguson, D. M., Radmer, R. J., Seibel, G. L., Singh, U. C., Weiner, P. K., and Kollman, P. A. (1997) AMBER 5.0, University of California, San Francisco, CA.
37. Wang, A., Ughetto, G., Quigley, G., and Rich, A. (1987) *Biochemistry 26*, 1152−1163.
38. Cheatham, T. E., and Kollman, P. E. (1996) *J. Mol. Biol. 259*, 434−44.
39. Pasternack, R. F., Giannetto, A., Pagano, P., and Gibbs, E. J. (1991) *J. Am. Chem. Soc. 113*, 7799−7800.
40. Kelly, J. M., Murphy, M. J., McConnell, D. J., and OhUigin, C. (1985) *Nucleic Acids Res. 13*, 167−84.
41. Banville, D. L., Marzilli, L. G., Strickland, J. A., and Wilson, W. D. (1986) *Biopolymers 25*, 1837−58.
42. Pasternack, R. F., Goldsmith, J. I., Szep, S., and Gibbs, J. E. (1998) *Biophys. J. 75*, 1024−1031.
43. Gandini, S. C. M., Borissevich, I. E., Perussi, J. R., Imasato, H., and Tabak, M. (1998) *J. Lumin. 78*, 53−61.
44. Borissevitch, I. E., and Gandini, S. C. M. (1998) *J. Photochem. Photobiol. B: Biol. 43*, 112−120.
45. Nussbaum, J. M., Newport, M. E. A., Mackie, M., and Leontis, N. B. (1994) *Photochem. Photobiol. 59*, 515−528.
46. Wuthrich, K. (1986) *NMR of Proteins and Nucleic Acids*, J. Wiley and Sons, Inc.
47. Schmitz, U., and James, T. L. (1995) *Methods Enzymol. 261*, 3−44.
48. Schmitz, U., and James, T. L. (1995) *Methods Enzymol. 261*, 3−44.
49. Schmitz, U., Pearlman, D. A., and James, T. L. (1991) *J. Mol. Biol. 221*, 271−92.
50. Ravinshaker, G. S., Swaminathan, D. L., Beveridge, R. L., and Sklenar, H. (1989) *J. Biomol. Struct. Dyn. 6*, 669−699.
51. Sandström, J. (1982) *Dynamic NMR Spectroscopy*, Academic Press, New York.
52. Trotta, E., D'Ambrosio, E., Ravagnan, G., and Paci, M. (1995) *Nucleic Acids Res. 23*, 1333−1340.
53. Trotta, E., D'Ambrosio, E., Grosso, N., Ravagnan, G., Girilli, M., and Paci, M. (1993) *J. Biol. Chem. 268*, 3944−3951.
54. Craik, D. J., Pavlopoulos, S., and Wickham, G. (1996) in *NMR in Drug Design* (Craik, D. J., Ed.) pp 423−464, CRC Press, Boca Raton, FL.
55. Weisz, K., James, T., and Shafer, R. (1992) *Eur. J. Biochem. 204*, 31−38.
56. Janson, T. R., and Katz, J. J. (1979) *The Porphyrins*, Vol. 4, Academic Press, Inc., New York.
57. Humphery, F. W., Dalke, A., and Shulten, K. (1996) *J. Mol. Graphics 14*, 33−38.

BI9913808